Strain induced crystallization and melting of natural rubber during dynamic cycles

*Nicolas Candau [a,b], Laurent Chazeau *[,a,b], Jean-Marc Chenal [a,b], Catherine Gauthier [c], José Ferreira [a,b], Etienne Munch [c], Dominique Thiaudière [d]*

[a] Université de Lyon, CNRS

[b] MATEIS, INSA-Lyon, CNRS UMR5510, F-69621, France

[c] Manufacture Française des Pneumatiques Michelin, Centre de technologies, 63040 Clermont Ferrand Cedex 9, France

[d] Synchrotron SOLEIL - Ligne de lumière DIFFABS, L'orme des merisiers, Saint Aubin, 91192 Gif sur Yvette, France

*Corresponding author: Laurent Chazeau, e-mail: laurent.chazeau@insa-lyon.fr

Keywords: strain-induced crystallization, natural rubber, in situ WAXS, self-heating

Abstract

Strain-induced crystallization (SIC) of natural rubber (NR) is studied during dynamic cycles at high frequency (with equivalent strain rates ranging from 7.2 s^{-1} to 290 s^{-1}). Different testing parameters are varied: the frequency, the temperature and the stretching ratio domain. It is found that an increase of the frequency leads to a decrease of the crystallinity during both loading and unloading steps of the cycle. Nevertheless, the interpretation of the curves needs to take into account several phenomena such as (i) an instability of the crystallites generated during the loading step, which increases with the frequency, (ii) the memory of the previous alignment of the chains, which depends on the minimum stretching ratio of the cycle λ_{min} and of the frequency, (iii) self-heating which makes more difficult the crystallites nucleation and easier

their melting. Thus, when the stretching ratio domain is above the expected stretching ratio at complete melting λ_{melt}, the combination of these phenomena leads, at high frequency, to unexpected results such as a complete melting at λ_{min}, and to an hysteresis in the CI-λ curves.

1. Introduction

The excellent mechanical properties of natural rubber (NR) are thought to be the consequence of its ability to crystallize under strain. In particular, there are ongoing works to understand the fracture [1, 2], crack growth [3-7] and fatigue behaviour [8, 9] of NR and their relationship with strain induced crystallization (SIC). This phenomenon was for the first time evidenced by Acken and Long [10, 11] only few years after the discovery of SIC in 1925 [12]. These pioneering works evidenced that SIC is a kinetic phenomenon which requires a very short time (less than one second) to occur when the rubber is stretched at a sufficiently high stretching ratio. For that reason, SIC kinetics remains difficult to characterize.

In literature, the strategy to study it has often been indirect, by the use of thermal [13-15] or mechanical measurements [16]. Unfortunately, these techniques provide only partial information, as they do not give access to the crystalline microstructure. The progressing ability of X-rays detectors has then been used to capture more and more rapidly a diffraction pattern. In particular, recent in situ WAXS experiments using impact tensile test [17, 18] allowed evaluating SIC process on a sample rapidly stretched and relaxed in the deformed state. These papers give interesting results concerning the kinetics of the incipient crystallites in the deformed state, but they do not allow performing measurement during the deformation of the sample.

The stroboscopic approach can be used to solve this problem. It allows recording WAXS patterns by accumulation of the diffracted intensity thanks to a stroboscopic acquisition. The advantages of such a technique are first to avoid any averaging over an elongation domain (since a stroboscopic device selects the desired elongation level), secondly to enable in situ WAXS measurements in a frequency range never reached before. With this technique, Kawai et al. [19] clearly evidenced that the crystallinity of a vulcanized natural rubber, measured during the dynamic cycles, decreases when frequency increases from 0.1 Hz to 10 Hz. More recently, Albouy et al. [20] used the same approach but in a larger frequency range (from 0.01 Hz to 50 Hz) and studied both crystallization and melting kinetics whose characteristic times were found

around several decades of milliseconds. We also published preliminary results showing how SIC kinetics accelerates with the stretching ratio [21]. However, these studies only focused on the SIC characteristics at the minimum and at the maximum stretching ratio reached during the dynamic cycle, and not on its evolutions in between these two values.

Thus, the present paper is dedicated to the study of SIC during a complete dynamic cycle at high frequencies thanks to the improvement of our stroboscopic device. The experimental procedure allows to completely follow both crystallization and melting processes of NR samples when stretched in conditions of solicitation similar to those met in usual applications (for instance in damping applications). A complete analysis of the crystalline features such as the crystallinity index (CI), the crystallites sizes (L_{hkl}), their orientation (ψ_{hkl}) is developed. Several loading and thermal conditions are explored thanks to various pre-stretching conditions and temperatures. This last parameter is known to be a major one that controls SIC in NR at "slow" strain rate [22, 23, 16]. Its effect on SIC during cycles at high stretching ratios and strain rates is especially discussed in the last section.

2. Materials and experiments

2.1. Materials

The samples composition is the following: NR rubber gum (Technically Specified Rubber TSR20) provided by Michelin Tire Company, stearic acid (2 phr, i.e. 2 g per 100 g of rubber), ZnO (1.5 phr), 6PPD (3 phr), CBS (1.9 phr) and sulfur (1.2 phr). The material has been processed following the Rauline patent [24]. First, the gum is introduced in an internal mixer and sheared for 2 min at 60°C. Then, the vulcanization recipe is added and the mix is sheared for 5 min. The material is afterward sheared in an open mill for five minutes at 60°C. Sample sheets are then obtained by hot pressing at 170°C during 13 min. Dumbbell-shaped samples, with a 6 mm gauge length (l_0) and 0.8 mm thickness, are machined. The average network chain density ν was estimated from the swelling ratio in toluene and from the Flory – Rehner equation [25] and found equal to 1.4×10^{-4} mol.cm^{-3}. This density is tuned so that (i) it promotes the development of strain-induced crystallization [26] and (ii) it is high enough to avoid an inverse yield effect [27]. In order to avoid microstructure modification during the different mechanical tests, i.e. an

uncontrolled Mullins effect, the samples are stretched four times up to stretching ratio (λ = 7) higher than the maximum stretching ratio reached during the in situ cyclic tests (λ = 6).

2.2. In situ WAXS measurements at slow strain rate

The in situ WAXS experiments are carried out on the D2AM beamline of the European Synchrotron Radiation Facility (ESRF). The X-ray wavelength is 1.54 Å. Tests consist of stretching a NR sample at a constant strain rate (4.2×10^{-3} s^{-1}) and at fixed temperature.

The two-dimensional (2D) WAXS patterns are recorded by a CCD camera (Princeton Instrument). The background, (i.e. air scattering and direct beam intensities) is properly measured in absence of any sample. It can then be subtracted to the total intensity scattered in the presence of the rubber sample. The corrected scattering intensity is finally normalized by the thickness and the absorption of the sample. Each scattering pattern is integrated azimuthally. The deconvolution of the curve $I=f(2\theta)$ enables the extraction of the intensity at the peak top and the width at half height of each crystalline peak and the intensity at the peak top of the amorphous phase. The crystallinity index CI is then determined as follows [28]:

$$CI = \frac{I_{a0} - I_{a\lambda}}{I_{a0}} \tag{1}$$

where I_{a0} and $I_{a\lambda}$ are the intensity of the amorphous phase at the peak top in the unstretched state and the stretched state, respectively. The average crystallite sizes L_{hkl} (L_{200}, L_{102} and L_{002}) in the direction normal to the (*hkl*) planes, are estimated from the Scherrer equation:

$$L_{hkl} = \frac{K\lambda_w}{\beta_{1/2} cos\theta} \tag{2}$$

where λ_w is the wavelength and θ is the Bragg angle. In this study, each crystalline peak is fitted with a Lorentzian function in which the width at half-height is $\beta_{1/2}$. According to the parameters chosen for the fit of the experimental peak, the K value is 0.64 [29]. In order to measure the average crystallite size in the stretching direction L_{002} (c_1), the tensile test machine is tilted by an angle around 10°.

The orientation of crystallites ψ_{hkl} is given by half width at half-height of the crystalline peak in the direction normal to the plane (hkl), integrated over the azimuth.

2.3. In situ WAXS measurements in dynamic conditions

The in situ WAXS measurements during dynamic cycles are carried out on the Diffabs beamline of the French national Synchrotron SOLEIL. A specifically dedicated apparatus was developed in order to perform WAXS measurements during high velocity cyclic tensile tests with large amplitude and high frequencies (up to 80 Hz) [21] (figure 1). Thanks to a stroboscopic acquisition, the diffraction pattern is not averaged over the whole cycle, but is acquired at a chosen stretching ratio. In addition, the temperature increase of the material, which can be significant at high frequencies and large amplitude, is also estimated during the test thanks to the measurement of the sample surface temperature with an Infra-Red pyrometer (CTLF-CF3-C3) of Microepsilon.

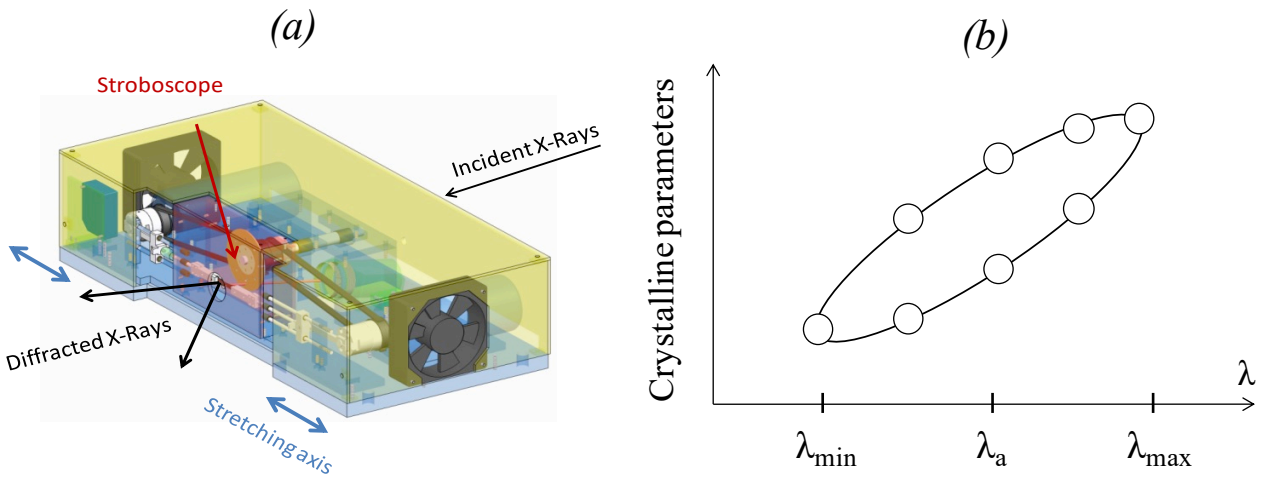

Figure 1. (a) View of the homemade machine. (b) Reconstruction of the "crystallinity cycle".

The stroboscopic acquisition of the WAXS pattern at the chosen stretching ratio is made so that the time of exposure is 1/44th of the time for a complete cycle. This means that a 1 sec exposure time at given elongation needs an acquisition over 44 cycles. The device enables to dynamically stretch the samples over a fixed amplitude $\Delta\lambda = \lambda_{max}-\lambda_{min}$ ranging from 0 to 2, around an average stretching ratio λ_a fixed at the beginning of the experiment. The testing procedure is the following: the NR sample is first rapidly pre-stretched at λ_a and let to relax in the deformed state during five minutes. Sample is then dynamically deformed around λ_a with the total amplitude $\Delta\lambda$

with an increasing frequency (from 2Hz to 80Hz). Once this sequence is finished, the sample is kept at λ_a during five minutes. During this relaxation phase, the aperture of the stroboscopic system is changed for another position. This procedure is repeated for 8 positions of the cycle, allowing measuring the crystalline parameters during the whole cycle (figure 1). In order to limit fatigue during the dynamic tests, each sample is submitted to only four dynamic sequences (four positions), i.e. two samples are used to describe the whole cycle.

Tests called hereafter A, B and C, are performed at room temperature, whereas tests E and F are performed at 50°C. Pre-stretching values λ_a are modified in order to perform cyclic tests above or below the melting stretching ratio λ_{melt}. This melting stretching ratio corresponds to the stretching ratio of complete melting of crystallites during unloading of a cyclic test performed at slow strain rate ($4.2 \times 10^{-3}\ s^{-1}$) and at a given temperature. The dynamic amplitude $\Delta\lambda$ is chosen equal to 1.8. This value is high enough to expect a significant variation of CI during the dynamic cycle. Indeed, if the amplitude is too low, the CI variations measured during the cycle are too weak (refer to figure 10 in the appendix).

3. Results

3.1. Influence of the stretching ratio domain

We first study the effect of the stretching ratio domain explored during dynamic cycles performed at room temperature and at 2 Hz (figure 2a). The cycle of a NR sample stretched at room temperature and at slow strain rate ($4.2 \times 10^{-3}\ s^{-1}$ equivalent to 10^{-3} Hz), so called hereafter "the reference curve" is added on the same figure. The loading conditions of these tests are given in figure 2a. Figure 2b presents the evolution of CI as a function of the stretching ratio domain. For the slow strain rate cycle (test D), the first crystallites appear during the loading step at $\lambda_{cryst} = 4.3$, so-called hereafter stretching ratio at SIC onset. During unloading, CI progressively decreases and the crystalline phase totally disappears at the melting stretching ratio $\lambda_{melt} = 3$. Concerning the dynamic tests, two cases can be distinguished: the cycle can be performed partly or totally above the melting stretching ratio λ_{melt} corresponding to the conditions $\lambda_{min} \leq \lambda_{melt}$ or $\lambda_{min} > \lambda_{melt}$ respectively. For dynamic tests A and B, SIC is poorly developed during the cycle and no hysteretic shape is observed. This is due to (i) a low λ_{max} value which avoids a strong increase of CI during loading and (ii) a low λ_{min} value which is below or equal to λ_m and thus leads to the

complete melting of crystallites during unloading. For test C, CI is strongly enhanced not only due to an increase of λ_{max} but also to the value of λ_{min}, which is now above λ_{melt}, avoiding the complete melting during unloading. In spite of a stretching ratio domain above λ_{melt}, a crystalline hysteresis is still observed. This is therefore different from what was observed during cyclic experiments at slow strain rate: Candau et al. [30] evidenced that, even after their melting, the chains of the crystallites keep the memory of their alignment, as far as the stretching ratio has not been decreased down to λ_{melt}. This eases crystallite nucleation during reloading, leading to the disappearance of the crystallinity hysteresis.

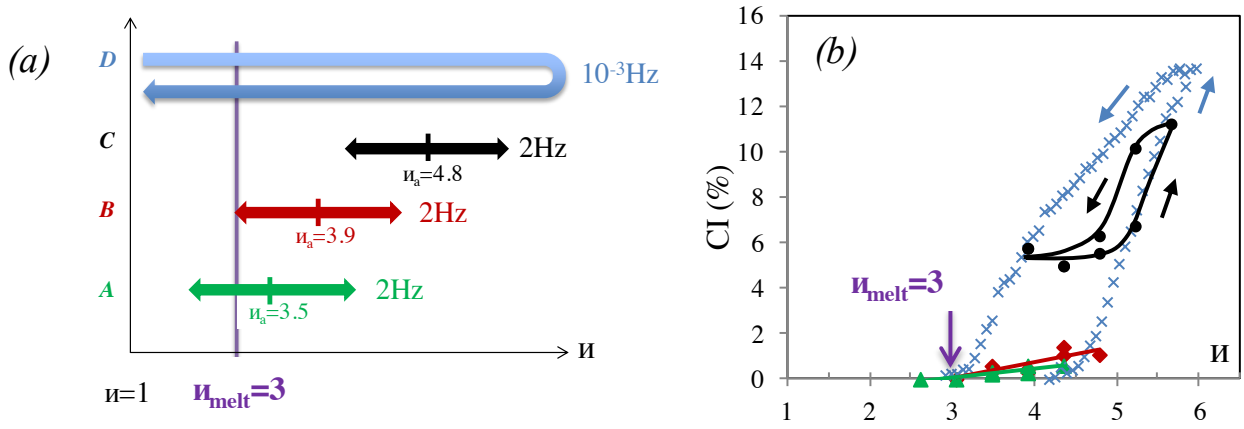

Figure 2. (a) Loading conditions of tests: A (λ_a=3.5), B (λ_a=3.9), C (λ_a=4.8) and D. (b) CI versus λ during the cycles: test A (triangle symbols), test B (diamond symbols), test C (circle symbols) and test D (cross symbols).

3.2. Influence of the frequency

The frequency of the dynamic cycles is now increased up to several decades. The temperature of the testing chamber is fixed at 21°C. For tests performed with $\lambda_{min} \leq \lambda_{melt}$, CI continuously decreases with the increase of the frequency (unpresented data). For the test performed above λ_{melt} (figure 3), when the frequency increases from 2 Hz to 5 Hz, the CI curve seems shifted to a lower value but its hysteretic shape is unchanged. At 10 Hz, CI suddenly falls. From 10 Hz to 40 Hz, CI continues to decrease and reaches zero at λ_{min}. The hysteretic shape is no more visible because of the low CI values measured. The CI cycles are then very similar to those observed during the tests performed with $\lambda_{min} \leq \lambda_{melt}$ in spite of the fact that the stretching ratio domain should be *a priori* always above λ_{melt}. Thus, the increase of the frequency might be equivalent to

an increase of λ_{melt}, the stretching ratio at complete melting. This will be further discussed in relation with the observed increase of the sample temperature with the frequency.

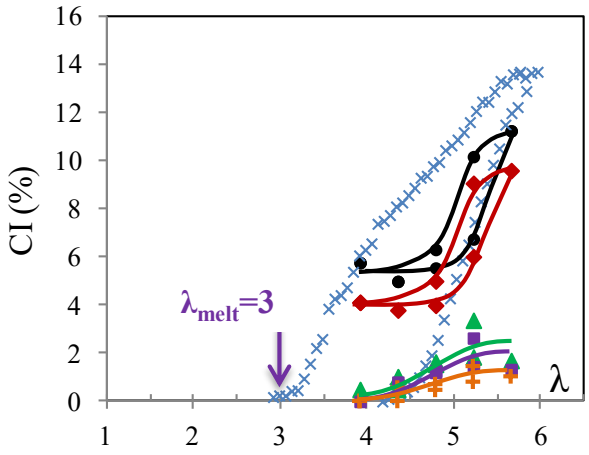

Figure 3. CI versus λ during test C performed at room temperature at 2 Hz (circle symbols), 5 Hz (diamond symbols), 10 Hz (triangle symbols), 20 Hz (square symbols) and 40 Hz (plus symbols). The slow strain rate cycle is added for comparison (cross symbols).

3.3. Influence of the ambient temperature

Whereas the previous tests were performed at room temperature, dynamic tests are now performed in an chamber whose temperature is fixed at 50°C (figure 4). Two cases are studied, one where $\lambda_{min} \leq \lambda_{melt\ (50°C)}$ and another where $\lambda_{min} > \lambda_{melt\ (50°C)}$ (tests E and F respectively), where $\lambda_{melt\ (50°C)}$ is now the melting stretching ratio of complete melting measured at slow strain rate and 50°C. As for the tests at room temperature: (i) for the lowest frequency, all crystallites melt during unloading in the case of the test E but not for the test F, (ii) when the frequency increases, CI decreases whatever the stretching ratio and CI at λ_{min} finally decreases down to zero, even for the test initially performed above $\lambda_{melt(50°C)}$.

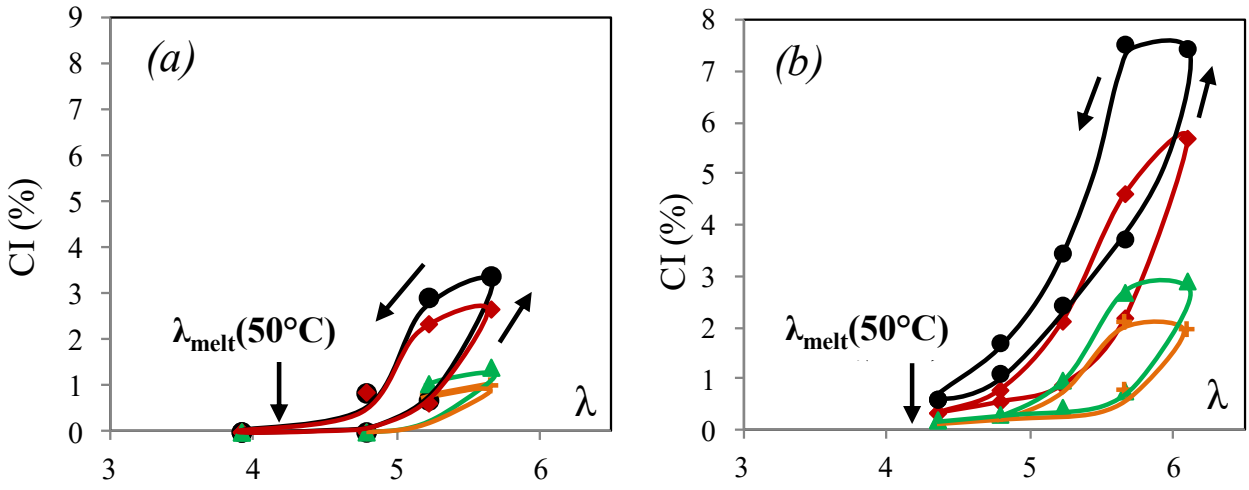

Figure 4. CI versus λ during dynamic tests: E (a) and F (b) performed at 2 Hz (circle symbols), 5 Hz (diamond symbols), 10 Hz (triangle symbols), and 40 Hz (plus symbols). Arrows indicate the direction of the cycles.

4. Discussion

The different results are complex to interpret as they depend on several interdependent parameters: temperature, frequency, and λ_{melt}. Moreover, as discussed below, different phenomenon involved in the strain-induced crystallization during dynamic cycles must be taken into account.

4.1. Strain rate and memory effects on crystallization

The hysteretic shape of the CI curve observed during the cyclic deformation at slow strain rate (test D, figure 2) is explained by the kinetic nature of the crystallization process which needs time to occur, whereas melting can be considered as instantaneous and the CI melting curves as representative of the thermodynamic equilibrium. Thus, due to the kinetics aspect of SIC, crystallization should depend on strain rate. This was evidenced by monotonic tests performed with strain rates varying from 4.2×10^{-3} s^{-1} (same strain rate than the reference cycle) to 2.8×10^{1} s^{-1} (similar strain rate than test C at 2 Hz) which show that the stretching ratio at SIC onset (λ_c) is delayed from 4.3 to 5.6 [31] (i.e. up to λ_{max} of our dynamic test C).Only knowing crystallization during a simple tensile test, we would have expected a crystallization onset at higher λ_c and therefore a lower CI at a given lambda. Thus, it is surprising to observe a similarity between the

crystallization curve during the loading of test C performed at 2 Hz and the reference crystallization curve (10^{-3} Hz) (figure 2b).

We must first consider the potential effect of the crystallinity build-up with the number of dynamic cycles. Beurrot et al. [8] followed the evolution of CI with time at λ_{max} during dynamic fatigue tests performed in very similar conditions than ours (cycles at 1 Hz with $\lambda_{min} > \lambda_{melt}$). After 4000 seconds (i.e. within an experimental time range similar to the one of our dynamic test), CI only increases of 1%. This increase is therefore too low to explain why the CI values measured during the loading step of the dynamic test C are so close to the ones of the reference crystallization curve.

In a previous paper [30], a cyclic test has been performed above λ_{melt} and at slow strain rate. The stabilised loading curve was found to be drastically shifted to lower stretching ratios compared to the reference crystallization curve. This was explained by a persistence of the chains alignment due to the memory of the chain orientation in the crystallite while the sample is not totally relaxed. This effect is indeed suppressed if the test is performed with $\lambda_{min} \leq \lambda_{melt}$. Thus the crystallinity developed during the loading step of the dynamic cycle performed at 2Hz and above λ_{melt} probably results from a combined effect of the high strain rate which should decrease CI at a given stretching ratio, and of this memory effect, which, conversely, increases CI, as illustrated in figure 5.

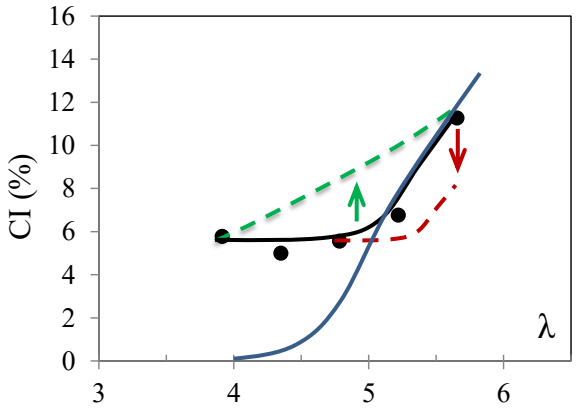

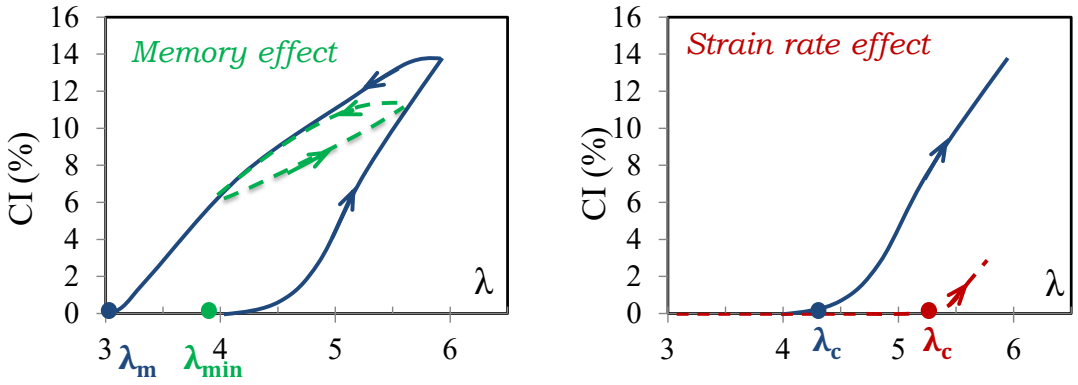

Figure 5. CI versus λ during the loading step of test C performed at 2 Hz and during the loading step of the slow strain rate cycle (test D). Scheme of the expected effects of the frequency increase and of the memory of the chains orientation in the crystallite.

4.2. Melting acceleration

The fact that the CI value measured at λ_{min} is the same at slow strain rate (during the unloading step) and at 2Hz is consistent with the scenario that each crystallite population involved in the dynamic cycle nucleates during the loading and completely melts during unloading. In other words, the measured CI at λ_{min} results from the summation of thermally stable crystallites (figure 6) which are not involved in the dynamic cycle and thus do not disappear as long as the temperature of the test is maintained constant. However, as commented previously, the shape of the CI curve during unloading of test C at 2 Hz (figure 2) suggests that melting is faster than during a cyclic test at slow strain rate (cf. for comparison the reference-melting curve). This indicates a weaker thermal stability of the crystallites created at high frequency. Same phenomenon was also observed on our filled NR samples [32] stretched in similar loading conditions.

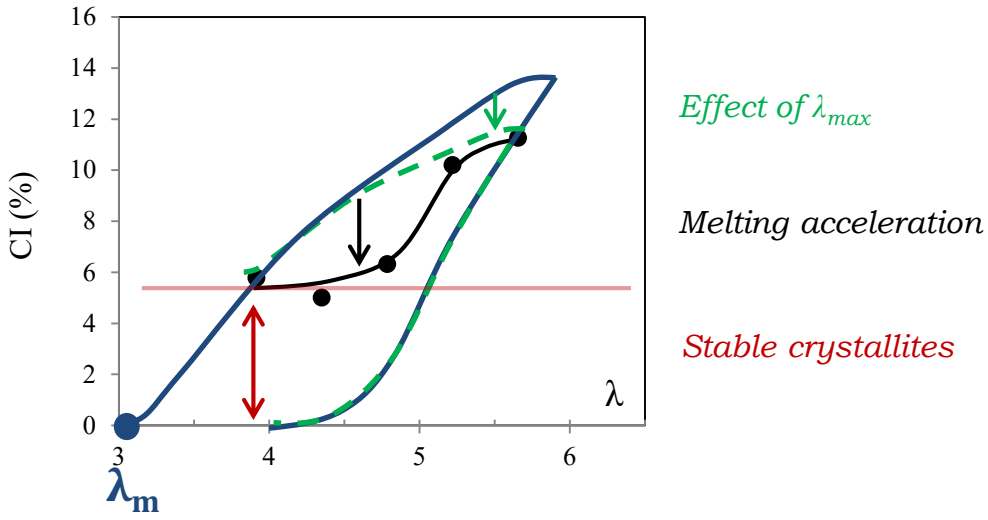

Figure 6. CI versus λ during the unloading step of test C performed at 2 Hz and during the unloading step of the slow strain rate cycle. Single arrow indicates the melting acceleration during unloading of test C and double arrow the CI at λ_{min} resulting from the accumulation of thermally stable crystallites.

The measurement of the crystallite dimensions and orientation could provide additional information on their stability. Figure 7a shows the orientation of the crystallites as a function of the stretching ratio for test C. The crystallites orient during the loading and slightly disorient during unloading, which is consistent with tests performed at slow strain rate [26, 33]. At a given stretching ratio, crystallites are slightly less oriented during unloading compared to loading, leading to a weak hysteresis. An increase of the frequency does not change the values of crystallite orientation: therefore, the orientation of the crystallites is only strain and not strain rate dependent.

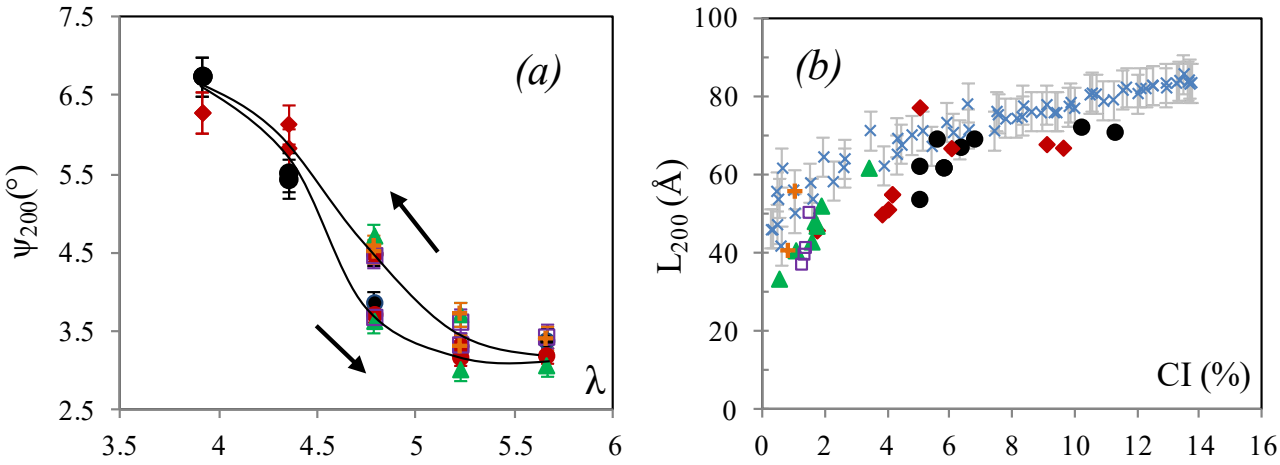

Figure 7. (a) Orientation of crystallites versus λ for test C performed at 2 Hz (circle symbols), 5 Hz (diamond symbols), 10 Hz (triangle symbols), 20 Hz (square symbols) and 40 Hz (plus symbols). (b) Corresponding L_{200} - CI curves. Arrows indicate the direction of the cycle. Lines are a guide for the eyes. The L_{200} - CI curve from test D is added (cross symbols).

The crystallite dimensions in the three principal directions (200), (120) and (002) of the orthorhombic structure of NR crystallites have been extensively studied during cyclic loadings at slow strain rates [26, 30, 33, 34]. According to these studies, the ratio between L_{120} and L_{200} is kept constant during loading or unloading phase. Moreover, the L_{002} is found roughly constant with the stretching ratio [26, 30]. The 1/3 ratio relationship between the two principal lateral crystallite sizes (L_{120} and L_{200}) was also found during our dynamic tests as well as the invariance with the stretching ratio of the size in the stretching direction (002). Thus, only the evolution of the size L_{200} will be discussed here: figure 7b presents its evolution as a function of CI for the dynamic test C (results obtained for the other dynamic tests are reported in appendix). For comparison, the evolution of L_{200} during the cycle at slow strain rate and room temperature (test D) is also plotted. The L-CI curves found during the dynamic tests are slightly below the one obtained during slow strain rate cycle. This suggests that the crystallites formed during fast cycle have almost reached their stabilised dimensions, and that the crystallite growth can still be considered as instantaneous compared to the experimental time. Thus, SIC kinetics is still rather controlled by nucleation. Nevertheless, the slightly lower L_{002} could indirectly indicate that the amorphous phase surrounding the crystallites is not in the same state as in the case of a much slower cyclic solicitation. Going further, the faster melting observed at high frequency might be due to the fact

that, when stretched at higher frequency, the amorphous chains surrounding the crystallites, in particular the topological constraints which are rejected from the crystallite, do not have the time to be properly relax. This could increase the interfacial energy of the crystallites and thus promote their melting. This would also explain a weaker memory effect and therefore the hysteresis of the CI-λ curves. Of course such interpretation would need further experimental evidences which are not in the scope of this study.

4.3. Self-heating

As shown on figures 3 and 4b, CI at λ_{min} for the tests performed above λ_{melt} (tests C and F) decreases with frequency. The most reasonable explanation is that the temperature of the test increases with frequency, leading to an increase of λ_{melt} increases. This is indeed the case, as shown on figure 8a where the surface temperature during test C is plotted as a function of the frequency. This self-heating (equal to $T_{surface} - T_i$, with T_i the ambient external temperature which is here equal to 21°C) is likely due to viscoelastic effects and thus logically increases with frequency.

In order to estimate more precisely the temperature influence on the melting stretching ratio λ_{melt}, a series of WAXS experiments has been performed at slow strain rate (4.2×10^{-3} s^{-1}) at different temperatures (diamond in figure 8b) and modeled with a thermodynamic approach (curve in figure 8b) proposed in a previous work [35]. From this evolution, assuming the equivalence between heat brought by self-heating and heat brought by an external source, the effect of self-heating on the melting stretching ratio can be evaluated for any given frequency.

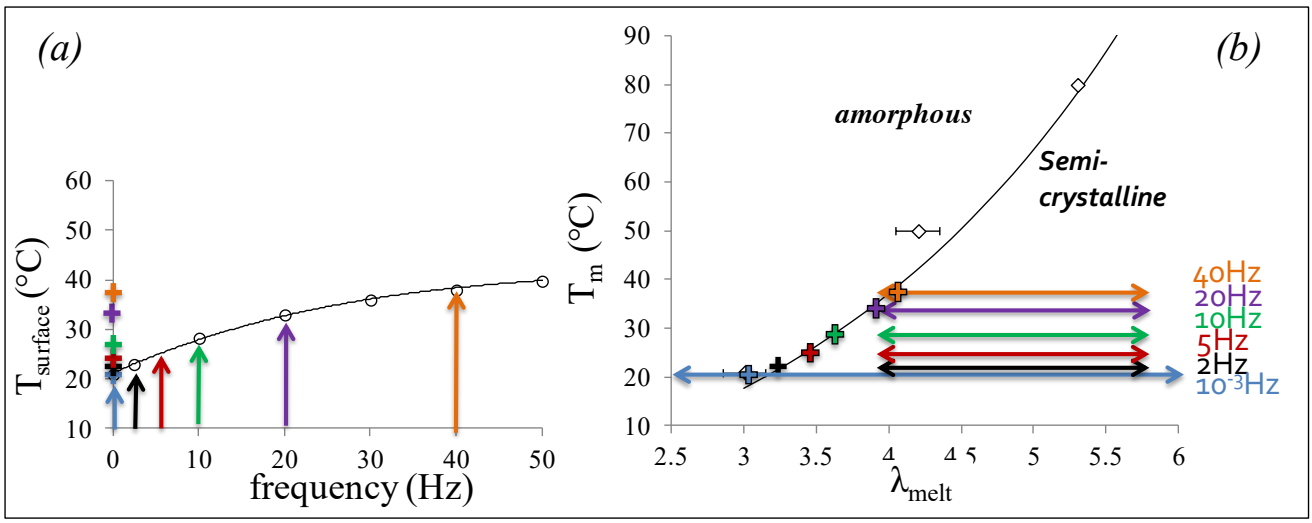

Figure 8. (a) Effect of the frequency on self-heating during test C and (b) relation between the melting temperature and the melting stretching ratio. Loading conditions of test D (double arrows) are added at the temperature corrected from self-heating measured for each frequency.

As shown in figure 3, the crystallinity at λ_{min} disappears at 20 Hz. This frequency is precisely the one for which λ_{melt} reaches the value λ_{min} because of self-heating (figure 8b). Same method has been applied to test F and leads to similar conclusions. Self-heating also decreases significantly the CI developed between λ_{min} and λ_{max} for two reasons: (i) the direct consequence of the increase of λ_{melt} above λ_{min} is a loss of the memory effect and therefore an increase of the nucleation time, (ii) this nucleation time is also directly increased by the temperature increase.

Indeed, as already shown in a large number of studies [16, 22, 23] with tensile tests experiments at slow strain rate (figure 9a), for higher temperature, the ability of NR to crystallize is weaker when temperature is increased. In particular, the stretching ratio at SIC onset λ_{cryst} is increased: the molecules must be more stretched in order to allow a sufficiently rapid nucleation within the time of the experiment. In other words, the strain energy (proportional to λ^2) must be higher, in order to compensate the larger enthalpic energy of crystallite formation [35].

The effect of the temperature can be directly shown by comparing dynamic tests C and E performed in same loading conditions, at 21°C and 50°C respectively (figure 9b), at 2 Hz since at this frequency, self-heating can be neglected (cf. figure 8b). During the loading step, the CI increase is weaker at 50°C. Compared to the curves obtained at slow strain rate, one must also

take into account the fact that at 50°C, λ_{melt} becomes lower than λ_{min}, leading also to a loss of the memory of the chain alignment during the unloading step, and therefore to a more difficult nucleation of the crystallites during the loading step.

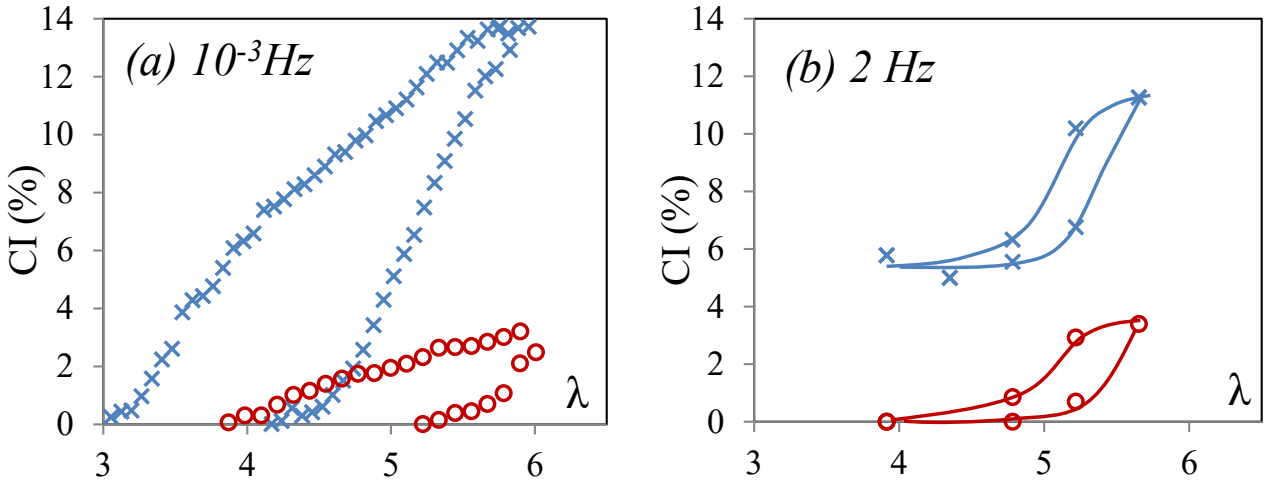

Figure 9. Crystallinity index as a function of the stretching ratio during (a) slow strain rate cycles at room temperature (test D) and 50°C, (b) dynamic test at 2 Hz at room temperature (test C) and 50°C (test E). Cross symbols are for tests performed at 21°C and circle symbols for tests performed at 50°C.

5. Conclusion

A dynamic tensile test machine recently developed was used in order to study strain-induced crystallization (SIC) of natural rubber (NR) during dynamic cycles at high frequency (with equivalent strain rates ranging from 7.2 s^{-1} to 290 s^{-1}). Different testing parameters have been studied: the frequency, the ambient temperature and the stretching ratio domain. As expected, in all cases, an increase of the frequency leads to a decrease of the SIC phenomenon during both the loading and the unloading steps. Nevertheless, the interpretation of the curves needed to take into account several phenomenon such as (i) an instability of the crystallites generated during the loading step, which increases with the frequency, (ii) the memory of the previous alignment of the chains, which depends on the minimum stretching ratio of the cycle λ_{min} and of the frequency, (iii) self-heating which makes more difficult the crystallites nucleation and easier their melting. Thus, when the stretching ratio domain is much above λ_{melt}, their combination leads at high frequency to unexpected results such as a complete melting at the lowest stretching

ratio of the cycle λ_{min}, and an hysteresis in the CI-λ curve. Obviously, these experimental data, and the complexity of the SIC that they highlight, strongly suggests that only physical model coupling the mechanics, the thermic and the thermodynamic will be able to provide a pertinent description of this phenomenon [36].

6. Acknowledgements

The authors are indebted to the synchrotron SOLEIL and the local contact Dominique Thiaudière for providing the necessary beamline time and technical assistance in the experiments on the DiffABS line.

7. Appendix

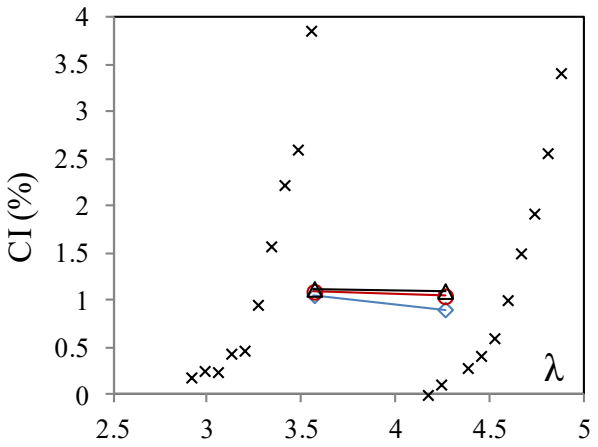

Figure 10. CI versus λ during a test performed with $\lambda_a = 4$ and $\Delta\lambda = 0.6$ and for the following frequencies: 2 Hz (diamond symbols), 5 Hz (circle symbols), 10 Hz (cross symbols).

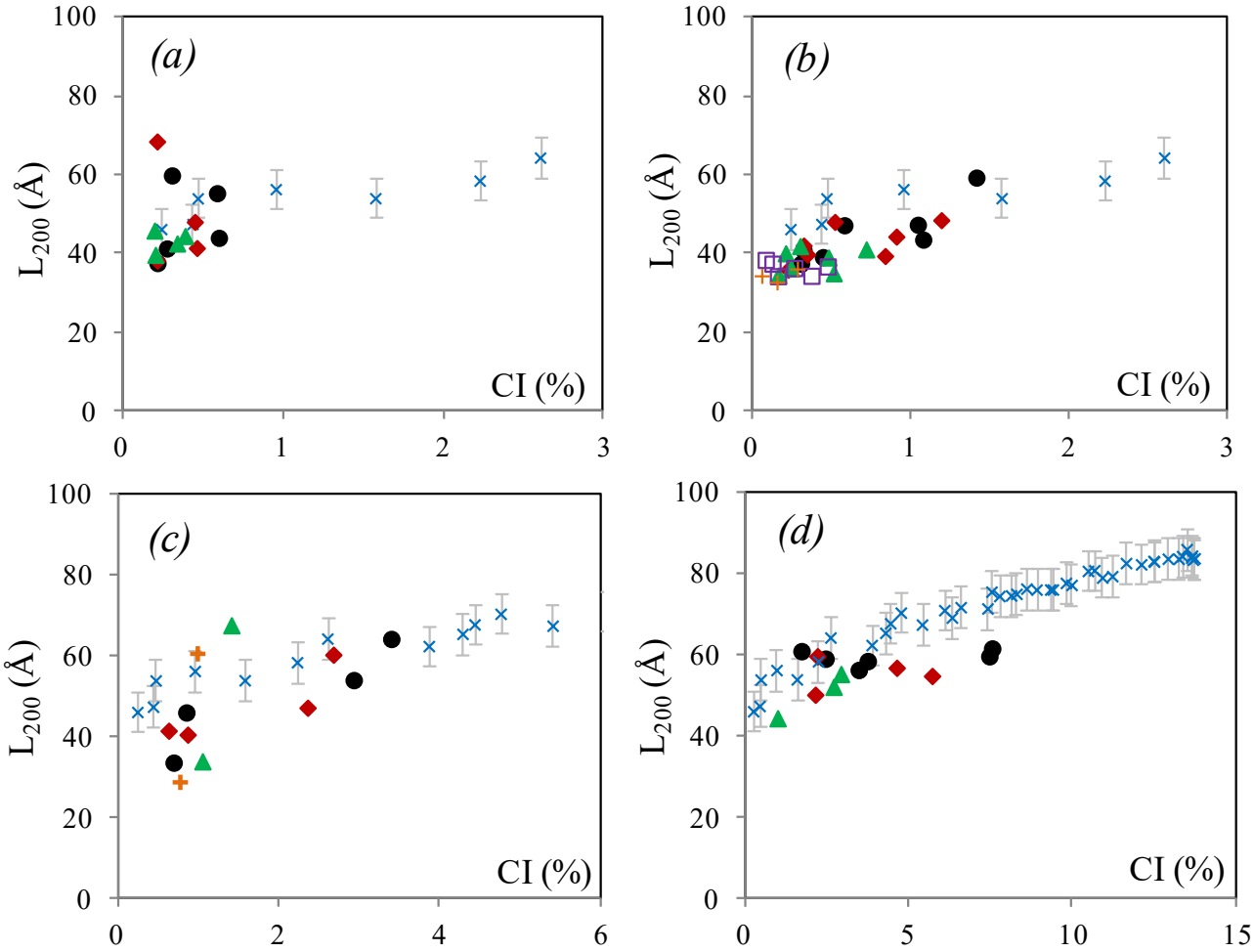

Figure 11. Crystallites size L_{200} versus CI for dynamic tests A (a), test B (b), test E (c) and test F (d) at different frequencies: 2 Hz (circle symbols), 5 Hz (diamond symbols), 10 Hz (triangle symbols), 20 Hz (square symbols) and 40 Hz (plus symbols). The L_{200} - CI curve from test D is added (cross symbols). For sake of clarity the error bar is given only for test at slow strain rate but same ones were estimated for dynamic tests.

8. References

1. L. González, J. L. Valentín, A. Fernández-Torres, A. Rodriguez and A. Marcos-Fernández, *Journal of Applied Polymer Science*., 2005, **98**, 1219-1223.

2. P. Y. Le Gac, M. Broudin, G. Roux, J. Verdu, P. Davies and B. Fayolle, *Polymer.*, 2014, **55**, 2535-2542.

3. P. Rublon, B. Huneau, N. Saintier, S. Beurrot, A. Leygue, E. Verron, C. Mocuta, D. Thiaudiere and D. Berghezan, *Journal of Synchrotron Radiation*., 2013, **20**, 105-109.

4. J. B. Le Cam and E. Toussaint, *Macromolecules*., 2010, **43**, 4708-4714.

5. S. Trabelsi, P. A. Albouy and J. Rault, *Macromolecules*., 2002, **35**, 10054-10061.

6. K. Bruning, K. Schneider, S. V. Roth and G. Heinrich, *Macromolecules*., 2012, **45**, 7914-7919.

7. J. S. Martinez, X. Balandraud, E. Toussaint, J. B. Le Cam and D. Berghezan, *Polymer.*, 2014, **55**, 6345-6353.

8. S. Beurrot-Borgarino, B. Huneau, E. Verron, and P. Rublon, *International Journal of Fatigue.*, 2013, **47**, 1-7.

9. N. Saintier, G. Cailletaud and R. Piques, *Materials Science and Engineering: A.,* 2011, **528**, 1078-1086.

10 J. D. Long, W. E. Singer and W. P. Davey, *Industrial & Engineering Chemistry.*, 1934, **26**, 543-547.

11 M. F. Acken, W. E Singer and W. Davey, *Industrial & Engineering Chemistry.*, 1932, **24**, 54-57.

12. J. R. Katz, *Naturwissenschaften*., 1925, **13**, 410-416.

13. J. R. S. Martinez, J. B. Le Cam, X. Balandraud, E. Toussaint and J. Caillard, *Polymer*., 2013, **54**, 2717-2726.

14. J. R. S. Martinez, J. B. Le Cam, X. Balandraud, E. Toussaint and J. Caillard., *Polymer*., 2013, **54**, 2727-2736.

15. J. C. Mitchell and D. J. Meier, *Journal of Polymer Science Part A-2: Polymer Physics*., 1968, **6**, 1689-1703.

16. Y. Miyamoto, H. Yamao and K. Sekimoto, *Macromolecules.,* 2003, **36**, 6462-6471.

17. M. Tosaka, K. Senoo, K. Sato, M. Noda and N. Ohta, *Polymer.,* 2012, **53**, 864-872.

18. K. Bruning, K. Schneider, S. V. Roth and G. Heinrich, *Macromolecules.,* 2012, **45**, 7914-7919.

19. H. Kawai, *Rheol. Acta.*, 1975, **14**, 27-47.

20. P. A. Albouy, G. Guillier, D. Petermann, A. Vieyres, O. Sanseau and P. Sotta, *Polymer*., 2012, **53**, 3313-3324.

21. N. Candau, L. Chazeau, J. M Chenal, C. Gauthier, J. Ferreira, E. Munch and C. Rochas, *Polymer*., 2012, **53**, 2540-2543.

22. J. Rault, J. Marchal, P. Judeinstein and P. A. Albouy, *Eur. Phys. J. E: Soft Matter Biol. Phys*., 2006, **21**, 243-261.

23. S. Toki, I. Sics, B. S. Hsiao, M. Tosaka, S. Poompradub, Y. Ikeda and S. Kohjiya, *Macromolecules*., 2005, **38**, 7064-7073.

24. Rauline, R. U.S. Pat., 5,227,425, 1993.

25. P. J. Flory and J. Rehner, *Journal of Chemical Physics*., 1943, **11**, 521-526.

26. J. M. Chenal, L. Chazeau, L. Guy, Y. Bomal and C. Gauthier, *Polymer*., 2007, **48**, 1042-1046.

27. P. A. Albouy, J. Marchal and J. Rault, *Eur. Phys. J. E: Soft Matter Biol. Phys*., 2005, **17**, 247-259.

28. G. R. Mitchell, *Polymer*., 1984, **25**, 1562-1572.

29. S. Trabelsi, S, Ph.D. Thesis, Université d'Orsay, Paris 11, 2002.

30. N. Candau, R. Laghmach, L. Chazeau, J. M. Chenal, C. Gauthier, T. Biben and E. Munch, *Macromolecules.*, 2014, **47**, 5815-5824.

31 N. Candau, R. Laghmach, L. Chazeau, J. M. Chenal, C. Gauthier, T. Biben and E. Munch, *European Polymer Journal.*, 2015, manuscript number: EUROPOL-D-14-01185R1.

32 N. Candau, L. Chazeau, J. M. Chenal, C. Gauthier and E. Munch, *Composites Science and Technology*., 2015, DOI:10.1016/j.compscitech.2014.12.014.

33 M. Tosaka, S. Murakami, S. Poompradub, S. Kohjiya, Y. Ikeda, S. Toki, I. Sics and B. S. Hsiao, *Macromolecules*., 2004, **37**, 3299-3309.

34 S. Trabelsi, P. A. Albouy and J. Rault, *Macromolecules*., 2003, **36**, 7624-7639.

35 N. Candau, R. Laghmach, L. Chazeau, J. M. Chenal, C. Gauthier, T. Biben and E. Munch, *Polymer.*, 2015, manuscript number: POLYMER-14-1644R1.

36 R. Laghmach, T. Biben, L. Chazeau and J.M Chenal, *Constitutive Models for Rubber VIII*, 2013, 473.